

Dynamical analysis and map modeling of a thermionic diode plasma experiment

C. Letellier^{a,*}, O. Ménard^a, Th. Klinger^b, A. Piel^c, G. Bonhomme^d

^a CORIA UMR 6614, Université de Rouen, Place Emile Blondel, F-76821 Mont Saint-Aignan Cedex, France

^b Institut für Physik, E.-M. Arndt Universität Greifswald, Domstr. 10a, D-17487 Greifswald, Germany

^c Institut für Angewandte und Experimentelle Physik, Christian-Albrechts-Universität, Olshausenstraße 40-60, D-24098 Kiel, Germany

^d LPMI-CNRS ESA 7040, Université Henri Poincaré, BP 239, F-54506 Vandœuvre-lès-Nancy Cedex, France

Received 15 February 2001; received in revised form 19 April 2001; accepted 19 April 2001

Communicated by F.H. Busse

Abstract

We perform a topological analysis of a chaotic behavior in a plasma experiment: a thermionic diode experiment. The stretching and folding mechanisms are schemed by a three branch template, i.e. a structure more complicated than the common horseshoe template. Moreover, a discrete model for the first-return map to a Poincaré section has been obtained from experimental data by using a global modeling technique. The template and the model give strong indications for a low dimension dynamics underlying the experimental data. © 2001 Elsevier Science B.V. All rights reserved.

PACS: 05.45.-a; 52.35.-g

Keywords: Map modeling; Thermionic diode plasma; Topological analysis

1. Introduction

When experimental data are investigated, it is an important task to determine whether the underlying dynamics can be described by a low-dimensional model. The most common way to answer this question is to compute a dimension of the attractor using a box-counting algorithm as introduced by Grassberger and Proccacia [1]. Nevertheless, although such a geometric invariant gives a first indication, more discriminating tools may be used. One of them is the topological analysis introduced by Mindlin et al. [2]

which provides a description of the structure of the flow as a branched manifold, often called a template or a knot-holder. The topological analysis procedure depends on identifying the stretching and squeezing mechanisms that are responsible for a chaotic attractor and which organize all the unstable periodic orbits embedded within the attractor in a unique way. The topological analysis procedure is reviewed in [3].

Most of the experimental dynamics investigated up-to-now are characterized by a two branch template associated with a quadratic map. Such a template is called a horseshoe template. One of them has been identified in a glow discharge experiment [4]. Nevertheless, very few experimental data have been associated with template, non-horseshoe, i.e. with a template having more than two branches. Let us

* Corresponding author. Tel.: +33-2-35-146557;
fax: +33-2-35-708384.
E-mail address: christophe.letellier@coria.fr (C. Letellier).

mention the cases of an electronic circuit [5], a laser system [6,7] or a Belousov–Zhabotinskii reaction [8]. When a non-horseshoe template is found, it becomes more constraining to find a model in agreement with the experimental data. This results from the fact that there are, basically, only two possibilities to have a dynamics corresponding to a two branch template, one associated with a quadratic map equivalent to the logistic map and one associated with a Lorenz-like map. On the contrary, many possibilities exist when a third branch is added.

The nonlinear dynamics of electric plasmas often leads to very complex behavior with many degrees of freedom. Nevertheless, there are situations where low-dimensional concepts apply and, for instance, methods of chaos control can be applied [9]. A particular example is simple plasma diodes, where global plasma oscillations may establish chaotic states due to internal memory effects caused by ion transit [10]. In the present work, experimental data from electron current fluctuations in a strongly driven thermionic plasma diode are analyzed by techniques borrowed from the nonlinear dynamical system theory. As a result, we obtain a discrete map that fits the experimental data very well. Of basic interest is the fact that the template associated with the phase space flow is found to be a non-horseshoe one, which has been observed in very few other experimental systems.

The paper is organized as follows. Section 2 describes the thermionic diode plasma experiment. Section 3 is devoted to the topological analysis of the experimental data and a discrete model is obtained for the first-return map in Section 4. Section 5 gives the conclusion.

2. The experiments

Periodic and chaotic oscillations have often been observed in periodically driven thermionic discharges [11]. The experiments were conducted by Mausbach et al. [12] in a cylindrical vacuum vessel (diameter 15 cm) with a filamentary tungsten cathode and an opposite anode plate made of stainless steel separated by a distance $L_d = 10$ cm (Fig. 1). A more-detailed description of the experiments and the physical mech-

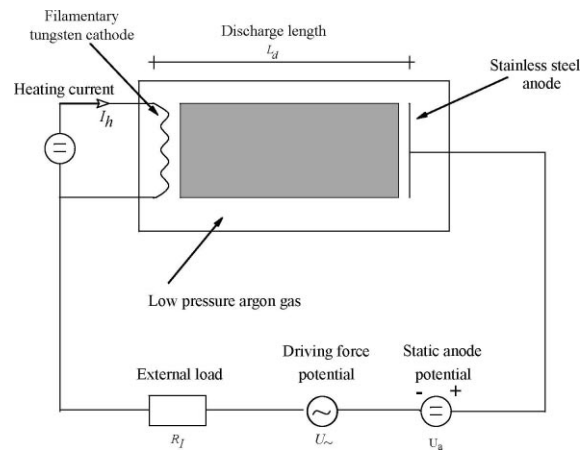


Fig. 1. Experimental set of the driven thermionic plasma diode.

anisms of the diode dynamics is given in Ref. [12]. The dynamical behavior of the diode depends on the static anode potential U_a to which is superimposed a sinusoidal driving potential in the range 5–30 V_{ss} . The external load R_l is chosen to be 100 Ω and the heating current I_h is equal to 4.2 A. In the case studied here, the argon gas is at a pressure $P_0 = 4 \times 10^{-1}$ Pa. Although the confinement of charged particles is fairly low, the discharge is self-sustained due to small surface-to-volume ratio. The driving force has an amplitude $U_\omega = 7.6 V_{ss}$.

A time series of the discharge current $I_d(t)$ is displayed in Fig. 2. It has been recorded with a transient digitizer of 12 bit vertical resolution. The length of the time series is usually 128 K. The sampling is either done stroboscopically (sampling at fixed phase with respect to the driver signal) when a first-return map is investigated (see Section 4) or the sampling rate was chosen sufficiently high to have roughly 10 data points per average period (in the present work typically 1–10 μ s).

3. Phase portrait analysis

This section is devoted to a topological analysis of the phase space flow underlying the time evolution of the current discharge. Data requirements for a topological analysis are conveniently expressed in terms

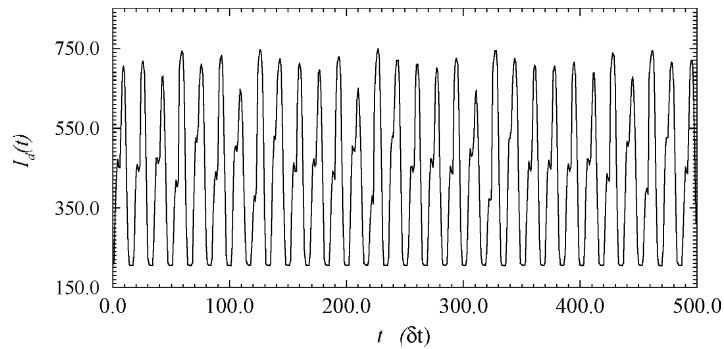


Fig. 2. Time evolution of the discharge current generated by a thermionic plasma diode.

of “cycles”. Roughly, a “cycle” is a revolution around the chaotic attractor; most often, it corresponds to a peak-to-peak oscillation of the recorded time series. As a matter of experience, a 100 cycles with 100 samples per cycle are sufficient [3]. When less than 50 samples per cycle are available, the data must be interpolated and/or smoothed in some way. In order to realize a spectrum-preserving interpolation, a Fourier method, based on zero padding of the direct Fourier Transform of the original time series as implemented in MATLAB, has been used. Thus, from the 10 samples per cycle, the interpolation procedure has been applied to have 100 samples per cycle. The data are then slightly smoothed over a window of one-fifth of the period.

From the preprocessed time series, a phase space is built by using derivative coordinates [13]. In order to do that, three derivative coordinates could be sufficient because the correlation dimension is slightly greater than 2 ($D_2 = 2.06$) [12]. The differential embedding is therefore spanned by

$$X(t) = I_d(t), \quad Y(t) = \frac{dI_d}{dt}, \quad Z(t) = \frac{d^2I_d}{dt^2}. \quad (1)$$

The derivatives are computed using a sixth degree interpolated polynomial. These interpolated polynomials are centered at each point by using the six nearest neighbors. Derivatives are then obtained by analytically differentiating these polynomials. A plane projection of the differential embedding is shown in Fig. 3.

Gilmore conjectured that it should be possible to propose a template as a schematic view of the phase portrait when the Lyapunov dimension obeys $2 \leq d_L < 3$, i.e. when a single Lyapunov exponent is positive [3]. Such a criterion results from the fact that the topological analysis method provides a caricature for the flow which vanishes all thickness in the transverse direction. The flow is thus described by a two-dimensional branched manifold where the two dimensions describe the direction of the flow and the direction of stretching. Since, in the present case, the Lyapunov dimension has been found to be equal to 2.08 [12], a template should well describe the flow associated with the time evolution of the discharge current.

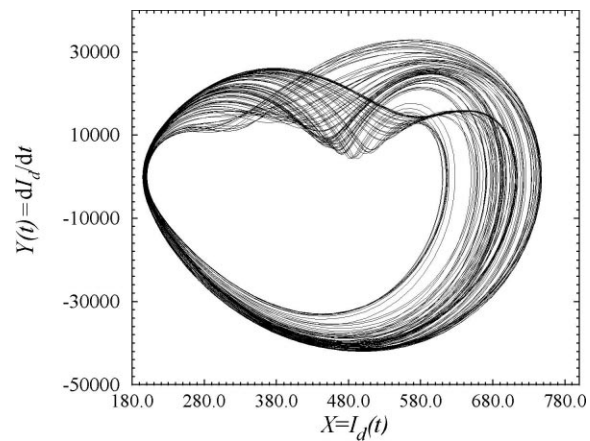


Fig. 3. Plane projection of the state portrait reconstructed by using the derivative coordinates.

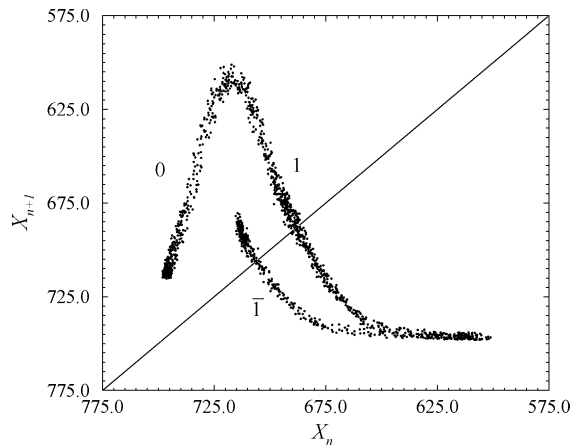


Fig. 4. First-return map to the Poincaré section P . Three monotonic branches may be identified.

The analysis starts by computing a first-return map to the Poincaré section

$$P \equiv \{(X_n, Z_n) \in \mathbb{R}^2 | Y_n = 0, Z_n < 0\}. \quad (2)$$

At first glance, the first-return map (Fig. 4) constitutes of two monotonic branches separated by a critical point located at the maximum. Nevertheless, the decreasing branch is layered and the topological analysis revealed that these monotonic branches have to be distinguished. The first-return map induces, therefore, a partition of the phase portrait in three regions. A symbol is associated with each branch. Chaotic trajectories and the periodic orbits constituting their skeleton are thus encoded over the symbol set $\{0, 1, \bar{1}\}$. The symbol “0” is associated with the increasing branch. The increasing branches are preserving order and decreasing branches are reversing order [14]. The phase portrait is necessarily divided into one preserving order strip and two reversing order strips. A preserving order strip represents an even number of half-turns, while a reversing order strip represents an odd number of half-turns. Consequently, the corresponding template will be composed of three strips. Periodic orbits may thus be encoded by symbolic strings. For instance, a period-2 orbit having one intersection with the Poincaré section located on the branch “0” and one located in the branch “1” is designated by the sequence (10). A period-3 orbit would have three symbols, and so on.

An adequate template must predict topological invariants like linking numbers between pairs of periodic orbits. A periodic orbit is here considered as a knot. Periodic orbits embedded within the attractor can be approximated by segments of the chaotic time series that mimic the behavior of nearby unstable periodic orbits. A “close return” method [17] is applied to the Poincaré section to extract them.

The linking numbers are ambient isotopy invariant defined as follows. Let α and β be two knots defining a link L in \mathbb{R}^3 . Let σ denotes the set of crossings of α with β . Then the linking number reads

$$lk(\alpha, \beta) = \frac{1}{2} \sum_{p \in \sigma} \varepsilon(p), \quad (3)$$

where ε is the sign of each crossing p with the usual convention, i.e.



The linking number $lk(\alpha, \beta)$ of two periodic orbits α and β is the half of the algebraic sum of all crossings between α and β (ignoring self-crossings).

From the experimental data, the linking numbers are counted on plane regular projections of orbit pairs by using the third coordinate to define the sign of crossings. For instance, orbits (1) and (10) are depicted in Fig. 5. This example is very simple and the linking number is found to be equal to -1 since three negative crossings and one positive crossing are identified. Nevertheless, we may encounter more ambiguous cases where oriented crossings are not so easily computed. Difficulties arise when segments of two different periodic orbits are close to tangency. In this case, spurious crossings may appear as displayed in Fig 6. Such spurious crossings may come from the preprocessing applied to the data since it is known that Fourier transform as used for oversampling the time series may imply additional oscillations. Without this filtering, however, the situation would be worst due to spurious crossings generated by noise contamination and the insufficient resolution of the trajectory. Consequently, we choose to remove by hand the spurious

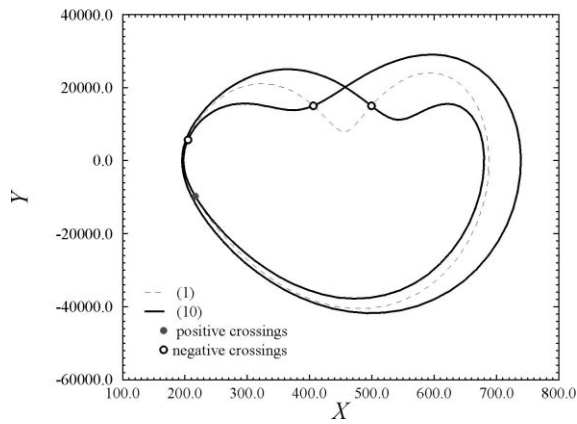


Fig. 5. Plane projection of a couple of periodic orbits encoded by (1) and (10), respectively. The associated linking number is equal to the half-sum of the oriented crossings, i.e. $lk(10, 1) = -1$.

crossings when required. Two cases of removal are observed. The first is displayed in Fig. 7.

Crossings are considered as spurious if they correspond to high frequency oscillations in the signal, i.e. frequencies large with respect to the frequency associated with the pseudo-period. In other terms, crossings between two strands may be considered as spurious when the distance between the crossings is smaller. In

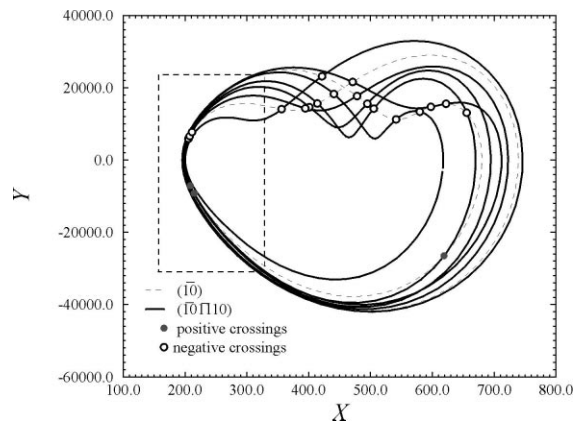


Fig. 6. Plane projection of a couple of periodic orbits encoded by $(\bar{1}0)$ and $(\bar{1}0\bar{1}10)$, respectively. The associated linking number is equal to the half-sum of the oriented crossings, i.e. $lk(\bar{1}0\bar{1}10, \bar{1}0) = -7$. The oriented crossings located in the box defined by the dashed line are not taken into account. Most of the time, the number of positive crossings is equal to the number of negative crossings. These crossings may be induced by the noise contamination of the experimental data.

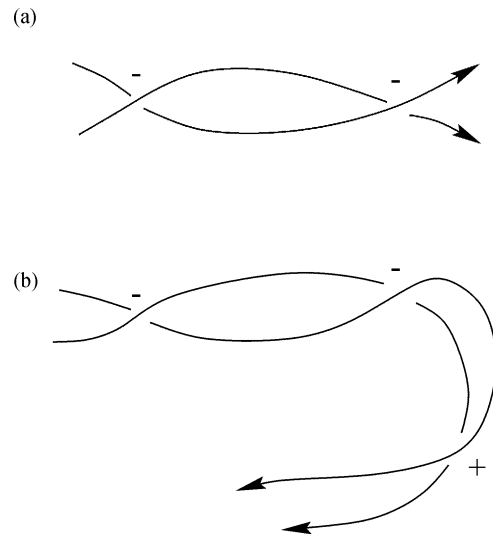


Fig. 7. Examples of spurious crossings which are removed, being considered as artifacts. In case (a), the relative positions of the two strands at the beginning and at the end of small interval are the same and the crossings are not taken into account. Conversely, case (b) corresponds to a situation where the relative position of the two strands are different, one negative crossing is therefore counted and the two close negative crossings are not considered as spurious since the two strands present a real crossing.

case of Fig. 7a, crossings are not taken into account since the relative positions of the two strands are the same. In case of Fig. 7b, the first two negative crossings are not considered as spurious since the relative positions of two strands is reversed and, consequently, the second negative crossing is vanished by the positive crossing under the assumption of isotopy. This removal procedure has been introduced by Lefranc and Glorieux [15] and later used by Boulant et al. [6,7] for processing experimental data generated by a laser system. The second case of removal correspond to the left part of the phase portrait where all the cycles are constrained in a thin tube. Noise contamination and pre-processing of the data induce a large number of spurious crossings. Nevertheless, in this region, the number of positive crossings is roughly equal to the number of negative crossings. The locations of these crossings clearly suggest that they result from “stochastic” process like noise contamination and not from a deterministic component of the dynamics. They are therefore ignored for computing the linking numbers.

Table 1

Linking numbers counted on plane projections of periodic orbits. They are found to be equal to those predicted by the template defined by the linking matrix (4)

lk	$(\bar{1}0)$	$(\bar{1}0\bar{1}1)$	$(\bar{1}0\bar{1}11)$	$(\bar{1}0\bar{1}110)$
(1)	-1	-2	-4	-3
$(\bar{1}0)$		-5	-6	-7
$(\bar{1}0\bar{1}1)$				-13

With this procedure, we find the linking numbers reported in Table 1. The linking number $lk(\bar{1}0\bar{1}1, \bar{1}0\bar{1}110)$ is not determined because the plane projection used does not allow to avoid any tangency over a long segment between these two periodic orbits. In such a case, it is not possible to count safely the oriented crossings. A template which can predict all computed linking numbers is described by the linking matrix

$$M_{ij} = \begin{bmatrix} -2 & -2 & -1 \\ -2 & -1 & -1 \\ -1 & -1 & -1 \end{bmatrix}, \quad (4)$$

according to the standard insertion convention [16]. The diagonal elements M_{ii} s are equal to the number of π -twists of the i th strip and off-diagonal elements M_{ij} ($i \neq j$) are given by the algebraic number of intersections between the i th and j th strips. The template associated with the linking matrix (4) is displayed in Fig. 8. Further details for such a topological characterization procedure are extensively discussed in [2,17].

The template obtained for this experimental data set is quite interesting because it is definitely different from the usual horseshoe map obtained in most of the cases studied elsewhere. The identification of this template is important for two reasons. First, when a layered first-return map is obtained (Fig. 4), we are not always ensured to be able to describe the dynamics by a template. Indeed, an attractor associated with a rather similar map has been obtained in a nine-dimensional Lorenz model [18] but it was impossible to find a template although the attractor has been successfully reproduced by a four-dimensional model obtained by using a global modeling technique from a scalar time

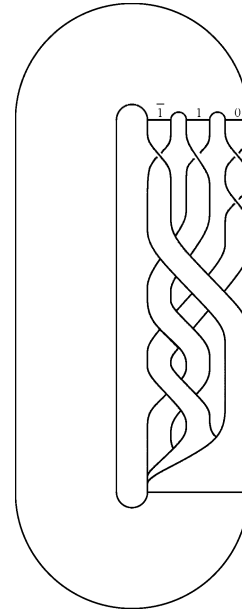


Fig. 8. Three strips template synthesizing the topological structure of the phase portrait of the experimental data recorded on the driven thermionic plasma diode.

series [18]. In the case of the thermionic diode experiment, the existence of the template displayed in Fig. 8 reveals that, although the underlying dynamics may be of a dimension higher than 3, the flow rapidly relaxes to a three-dimensional subspace of the phase space. Second, if a global model is obtained, it must generate a chaotic attractor characterized by the same template than the one here extracted from the data.

4. Map modeling

A thin tube in which all the trajectories are passing is observed in the phase portrait (Fig. 3). These segments of trajectories correspond to the long time interval Δt on which the current remains almost constant, the result of a relaxation process in the plasma discharge [19]. As a consequence, a given point in the reconstructed phase space may have two different “futures” and a deterministic model cannot be expected meaning that flow modeling is hopeless. It does not imply that it is not possible to find a set of

ordinary differential equations which captures the dynamics underlying the experimental data. Indeed, there exists some low-dimensional models which generate attractors presenting some regions of the phase space where all revolutions are sufficiently confined to be not distinguishable as soon as the time series are discretized or contaminated by noise. See, for instance, the six-dimensional model proposed by Lopes and Chian [21]. This is precisely the case of the thermionic diode dynamics. In this case, it is not possible to recover the differential structure from a single scalar time series. Such a lack of observability has been noted for the very simple Rössler system when the z -variable is considered as the physical quantity to measure [20]. Thus, the set of ordinary differential equations which must exist is not necessarily very complicated but one of the dynamical variable must remain nearly constant during a significant time interval. Let us insist that such a feature is quite characteristic of relaxation processes.

4.1. Map modeling technique

Nevertheless, a map modeling for the first-return map to the Poincaré section can be attempted. We consider maps reading as

$$\mathbf{X}_{n+1} = \mathbf{G}(\mathbf{X}_n), \tag{5}$$

where \mathbf{X}_{n+1} is the state vector at the $(n+1)$ th iteration ($n = 0, 1, \dots$) and \mathbf{G} defines the map under consideration. For an m -dimensional state vector, the system (5) involves m functions G_i which are assumed to be unknown. The aim is thereafter to obtain approximations \tilde{G}_i to the functions G_i s, from a time series made of consecutive values of one of the variables spanning the Poincaré section. Let x_n designate this variable.

The problem of approximating functions with a basis of polynomials starting from a time series has already been discussed for the case of flow modelings [22–26]. The approximation is then obtained by using a least-square method to minimize a quadratic error function which compares actual values of the function and approximated values. The functions are approximated by using multivariate monomial expansions on nets [26,27]. Similarly, in the case of map modeling,

the functions G_i s can be approximated by using polynomials. The approximation \tilde{G}_i to G_i then reads

$$\tilde{G}_i = \sum_{j=1}^{N_K} K_{ij} P^j, \tag{6}$$

where the P^j are monomials given by

$$P^j = x^k y^l z^m$$

in the three-dimensional case, with a biunivocal relationship between integers j and triplets (k, l, m) as defined in Ref. [26]. N_K is the number of monomials retained in the approximation. Here, x , y and z are equal to x_n , x_{n+1} and x_{n+2} , respectively. Sometimes rational functions are required to capture stiff variations observed on maps such as the Lorenz map or the four branches Rössler map investigated in Ref. [28].

The quality of the model depends on the following modeling parameters:

- N_c , the number of centers taken into account to approximate the model functions G_i s;
- N_K , the number of polynomials retained for estimating the model functions.

The models will be validated by using a probability density function of visits as introduced in Ref. [29].

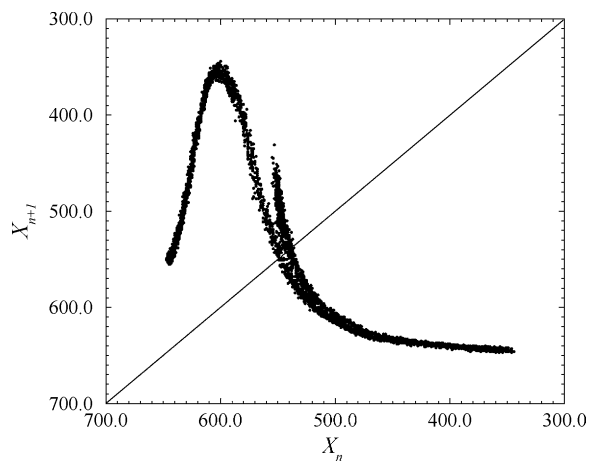


Fig. 9. First-return map of the stroboscopically sampled current oscillations.

4.2. Application to the experimental data

In this section, we are interested in modeling the underlying dynamics that governs an experimental data set described in terms of a discrete map. Rather than using a Poincaré section of the reconstructed phase portrait, we took advantage of the fact that the dynamical behavior is synchronized with a periodic driving force. The stroboscopically recorded current oscillations with respect to the driving force frequency allow

Table 2

Estimated coefficients K_p for the model function G obtained from the experimental time series recorded on the driven thermionic plasma diode. A single set of coefficients $K_{1,j}$ is reported because a single function G_1 is sufficient to capture the dynamics of the plasma experiment investigated here

j	k	l	$K_{1,j}$
1	0	0	10.546201806079
2	1	0	261.19848372722
3	0	1	-120.50124199277
4	2	0	-3193.6301117133
5	1	1	-2371.2376381203
6	0	2	643.83524189205
7	3	0	12676.456774224
8	2	1	26542.039539416
9	1	2	7463.7108381248
10	0	3	-1832.2376254873
11	4	0	-24587.109662417
12	3	1	-85834.002582640
13	2	2	-81632.619613464
14	1	3	-8764.0445047406
15	0	4	2736.5145406744
16	5	0	25546.115911921
17	4	1	123753.26307503
18	3	2	208991.02531978
19	2	3	111581.16147273
20	1	4	848.55188767912
21	0	5	-1973.4458152169
22	6	0	-13710.573357592
23	5	1	-83564.627967549
24	4	2	-203095.39550316
25	3	3	-212120.25275997
26	2	4	-64030.074970727
27	1	5	4242.3588757914
28	0	6	535.46451876984
29	7	0	2997.3869579818
30	6	1	21596.677621816
31	5	2	67421.841202925
32	4	3	108579.29108430
33	3	4	72382.159576379
34	2	5	11449.201058874
35	1	6	-1722.4053529534

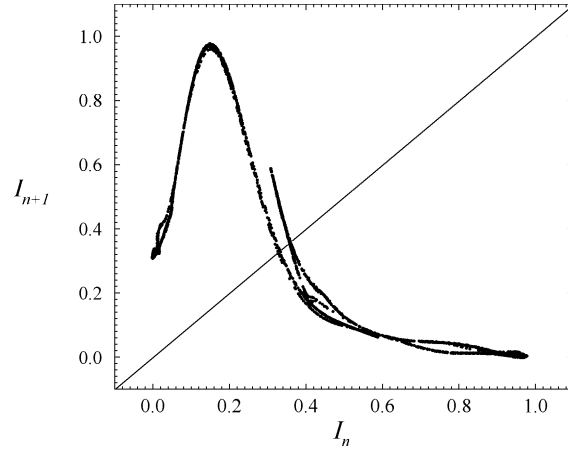


Fig. 10. First-return map generated by the model obtained from the experimental data.

one to define a first-return map to a Poincaré section of the dynamics (Fig. 9).

The best model has been obtained by using a polynomial form for a single model function G with the modeling parameters $(N_c, N_K) = (155, 35)$. Two coordinates are involved,

$$x_{n+2} = \tilde{G}(x_n, x_{n+1}). \quad (7)$$

The model constitutes of 35 monomials with a degree less than or equal to 7. The model coefficients are compiled in Table 2. The outcome of the model for the experimental first-return map is shown in Fig. 10. Its global shape is very similar to the shape of the experimental first-return map (Fig. 9). Nevertheless, the thickness of the model map is less important than for the experimental map. Such a discrepancy may arise from the noise contamination of the experimental dynamical behavior which is not captured by our deterministic model.

In order to have a better validation than visual inspection, a probability density function of visits [29] is computed. Such an invariant is very efficient for validating discrete models [28]. In the present case, the probability density function of visits (Fig. 11) is very similar for both the model and the experimental first-return map.

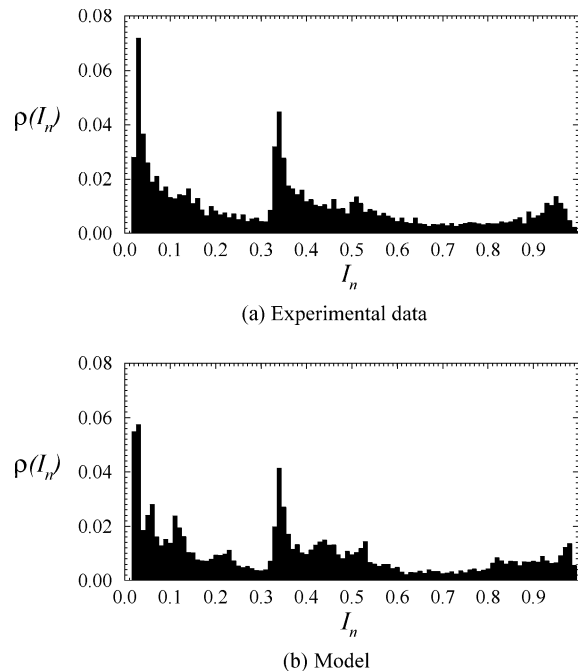


Fig. 11. Probability density functions of visits computed from the experimental data and synthetic data generated by the discrete model.

5. Conclusion

The chaotic attractor generated by a thermionic diode plasma experiment has been investigated in terms of a branched manifold schemed by a template. The dynamics is more complicated than the trivial horseshoe template. As a consequence, this dynamics may be described by a low-dimensional set of ordinary differential equations. Unfortunately, a lack of observability of the dynamics does not allow to obtain such differential equations by using a global modeling technique.

Indeed, the inverse modeling of the nonlinear dynamics of plasmas is a challenging task. In the present case, the stroboscopically recorded first-return map to a Poincaré section is sufficiently simple to be successfully modeled. The discrete model developed in the present paper is useful, for instance, for a deeper theoretical analysis of the control of its chaotic dynamics, as experimentally demonstrated in Ref. [19]. Future

work will be devoted to more complex situations which may have an immediate application like a more stable discharge behavior or improved plasma confinement owing to reduced chaotic particle transport.

References

- [1] P. Grassberger, I. Procaccia, Measuring the strangeness of strange attractors, *Physica D* 9 (1983) 189–208.
- [2] G.B. Mindlin, H.G. Solari, M.A. Natiello, R. Gilmore, X.J. Hou, Topological analysis of chaotic time series data from the Belousov–Zhabotinskii reaction, *J. Nonlin. Sci.* 1 (1991) 147–173.
- [3] R. Gilmore, Topological analysis of chaotic dynamical systems, *Rev. Mod. Phys.* 70 (4) (1998) 1455–1529.
- [4] T. Braun, R.R.B. Correia, N. Altmann, Topological model of homoclinic chaos in a glow discharge, *Phys. Rev. E* 51 (5) (1995) 4165–4168.
- [5] C. Letellier, G. Gouesbet, N. Rulkov, Topological analysis of chaos in equivariant electronic circuits, *Int. J. Bifurc. Chaos* 6 (12B) (1996) 2531–2555.
- [6] G. Boulant, M. Lefranc, S. Bielawski, D. Derozier, Horseshoe templates with global torsion in a driven laser, *Phys. Rev. E* 55 (5) (1997) 5082–5091.
- [7] G. Boulant, M. Lefranc, S. Bielawski, D. Derozier, A non-horseshoe template in a chaotic laser model, *Int. J. Bifurc. Chaos* 8 (5) (1998) 965–975.
- [8] C. Letellier, J. Maquet, H. Labro, L. Le Sceller, G. Gouesbet, F. Argoul, A. Arnéodo, Analyzing chaotic behaviour in a Belousov–Zhabotinskii reaction by using a global vector field reconstruction, *J. Phys. Chem. A* 102 (1998) 10265–10273.
- [9] T. Klinger, Control of chaos in plasmas, in: H.G. Schuster (Ed.), *Handbook of Chaos Control*, VCH/Wiley, Weinheim, 1999, pp. 513–562.
- [10] F. Greiner, T. Klinger, H. Klostermann, A. Piel, Experiments and particle-in-cell simulation on self-oscillations and period-doubling in thermionic discharges at low pressure, *Phys. Rev. Lett.* 70 (20) (1993) 3071–3074.
- [11] P.Y. Chang, A.Y. Wing, *Phys. Rev. Lett.* 59 (1987) 551.
- [12] T. Mausbach, T. Klinger, A. Piel, Chaos and chaos control in a strongly driven thermionic plasma diode, *Phys. Plasmas* 6 (10) (1999) 3817–3823.
- [13] N.H. Packard, J.P. Crutchfield, J.D. Farmer, R.S. Shaw, Geometry from a time series, *Phys. Rev. Lett.* 45 (9) (1980) 712–716.
- [14] P. Bergé, Y. Pomeau, Ch. Vidal, *L'ordre dans le Chaos*, Hermann, Paris, 1984.
- [15] M. Lefranc, P. Glorieux, Topological analysis of chaotic signals from a CO₂ laser with modulated losses, *Int. J. Bifurc. Chaos* 3 (3) (1993) 643–650.
- [16] P. Melvin, N.B. Tufillaro, Templates and framed braids, *Phys. Rev. A* 44 (6) (1991) 3419–3422.
- [17] C. Letellier, P. Dutertre, B. Maheu, Unstable periodic orbits and templates of the Rössler system: toward a systematic topological characterization, *Chaos* 5 (1) (1995) 271–282.

- [18] P. Reiterer, C. Lainscsek, F. Schürer, C. Letellier, J. Maquet, A nine-dimensional Lorenz system to study high-dimensional chaos, *J. Phys. A* 31 (1998) 7121–7139.
- [19] F. Greiner, T. Klinger, A. Piel, Nonlinear dynamical behavior of thermionic filamentary low pressure discharges. Part I. Simulation, *Phys. Plasmas* 2 (6) (1995) 1810–1821.
- [20] C. Letellier, J. Maquet, L. Le Sceller, G. Gouesbet, L.A. Aguirre, On the non-equivalence of observables in phase space reconstructions from recorded time series, *J. Phys. A* 31 (1998) 7913–7927.
- [21] S.R. Lopes, A.C.L. Chian, Controlling chaos in nonlinear three-wave coupling, *Phys. Rev. E* 54 (1) (1996) 170–174.
- [22] J.P. Crutchfield, B.S. McNamara, Equations of motion from a data series, *Complex Syst.* 1 (1987) 417–452.
- [23] R. Brown, N.F. Rul'kov, E.R. Tracy, Modeling and synchronizing chaotic systems from experimental data, *Phys. Lett. A* 194 (1994) 71–76.
- [24] M. Giona, F. Lentini, V. Cimagalli, Functional reconstruction and local prediction of chaotic time series, *Phys. Rev. A* 44 (6) (1991) 3496–3502.
- [25] G. Gouesbet, J. Maquet, Construction of phenomenological models from numerical scalar time series, *Physica D* 58 (1992) 202–215.
- [26] G. Gouesbet, C. Letellier, Global vector field reconstruction by using a multivariate polynomial L_2 -approximation on nets, *Phys. Rev. E* 49 (6) (1994) 4955–4972.
- [27] C. Letellier, L. Le Sceller, P. Dutertre, G. Gouesbet, Z. Fei, J.L. Hudson, Topological characterization and global vector field reconstruction from an experimental electrochemical system, *J. Phys. Chem.* 99 (1995) 7016–7027.
- [28] O. Ménard, C. Letellier, J. Maquet, G. Gouesbet, Modeling maps by using rational functions, *Phys. Rev. E* 62 (5) (2000) 6325–6331.
- [29] E. Ott, *Chaos in Dynamical System*, Cambridge University Press, Cambridge, 1993.